

Constraining Hamiltonians from chiral effective field theory with neutron-star data

Cassandra L. Armstrong,^{1, 2} Brendan T. Reed,³ Tate Plohr,⁴
Henrik Rose,⁵ Soumi De,³ Rahul Somasundaram,³ and Ingo Tews³

¹*Facility for Rare Isotope Beams, Michigan State University, East Lansing, Michigan 48824, USA*^{*}

²*Intelligence and Space Research Division, Los Alamos National Laboratory, Los Alamos, NM 87545, USA*

³*Theoretical Division, Los Alamos National Laboratory, Los Alamos, NM 87545, USA*

⁴*Los Alamos High School, Los Alamos, NM 87544, USA*

⁵*Institut für Physik und Astronomie, Universität Potsdam,
Haus 28, Karl-Liebknecht-Str. 24/25, 14476, Potsdam, Germany*

(Dated: January 12, 2026)

Multi-messenger observations of neutron stars (NSs) and their mergers have placed strong constraints on the dense-matter equation of state (EOS). The EOS, in turn, depends on microscopic nuclear interactions that are described by nuclear Hamiltonians. These Hamiltonians are commonly derived within chiral effective field theory (EFT). Ideally, multi-messenger observations of NSs could be used to directly inform our understanding of EFT interactions, but such a direct inference necessitates millions of model evaluations. This is computationally prohibitive because each evaluation requires us to calculate the EOS from a Hamiltonian by solving the quantum many-body problem with methods such as auxiliary-field diffusion Monte Carlo (AFDMC), which provides very accurate and precise solutions but at a significant computational cost. Additionally, we need to solve the stellar structure equations for each EOS which further slows down each model evaluation by a few seconds. In this work, we combine emulators for AFDMC calculations of neutron matter, built using parametric matrix models, and for the stellar structure equations, built using multilayer perceptron neural networks, with the PyCBC data-analysis framework to enable a direct inference of coupling constants in an EFT Hamiltonian using multi-messenger observations of NSs. We find that astrophysical data can provide informative constraints on two-nucleon couplings despite the high densities probed in NS interiors.

Introduction. Neutron-star (NS) cores explore densities far larger than those in the center of atomic nuclei, providing unique opportunities to test theories of strong interactions [1–3]. The properties of NSs, such as their radii, masses, and tidal deformabilities, depend on microscopic interactions between nucleons at densities up to a few times the nuclear saturation density $n_0 \simeq 0.16 \text{ fm}^{-3}$ and, possibly, between exotic degrees of freedom at higher densities. Multi-messenger observations of NS properties can, therefore, directly inform our understanding of these interactions.

Modern nuclear interactions are described by Hamiltonians derived within chiral effective field theory (EFT), which provides a systematic expansion of nuclear forces in powers of the average nucleon momenta p over a breakdown scale Λ_b [4, 5]. Chiral EFT Hamiltonians depend on a set of low-energy couplings (LECs) which determine the strength of individual operator structures that appear at different orders in this expansion. In the two-nucleon (NN) sector, these LECs are typically adjusted to NN scattering data by solving the quantum-mechanical scattering problem [6–12]. In the three-nucleon (3N) sector, the LECs are usually fit to ground-state properties of light nuclei or the triton β decay [13–20], but different fit protocols have been proposed [21, 22]. The chiral EFT Hamiltonians are then employed in predictive calculations of larger quantum many-body systems, such as

medium-mass to heavy atomic nuclei [22–31] or dense nuclear matter [16, 19, 32–38].

Terrestrial nuclear systems, however, only explore small neutron-to-proton asymmetries and densities of the order of n_0 . Matter in NSs, in contrast, is very isospin-asymmetric and probes much larger densities. Adjusting nuclear forces and their LECs to properties of NS matter would provide valuable complementary constraints [39–42]. In this work, we explore how well data from NS mass measurements [43–45] from a gravitational-wave (GW) observation of two merging NSs, GW170817 [46], and from the Neutron Star Interior Composition Explorer (NICER) telescope [47–50] enable us to constrain the relevant LECs in a nuclear Hamiltonian from chiral EFT at next-to-next-to-leading order ($N^2\text{LO}$) in neutron matter.

Approach. To extract LECs from NS observations, our goal is to employ Bayesian inference to analyze astrophysical data. Bayesian inference necessitates millions of model evaluations, and hence, it requires us to be able to rapidly connect LECs with NS observables. To date, this connection is too computationally expensive. First, it requires solving the quantum many-body problem to obtain the dense-matter EOS from a given set of LECs, a process which costs 100,000’s of CPU hours per EOS. Second, NS observables are calculated from an EOS by solving the Tolman-Oppenheimer-Volkoff (TOV) equations, which takes a few seconds per EOS. These two steps are prohibitively slow for Bayesian inference; typically, likelihood evaluations need to be performed in less than $\sim 1\text{ s}$ [51]. Therefore, reducing this computational

* armst520@msu.edu

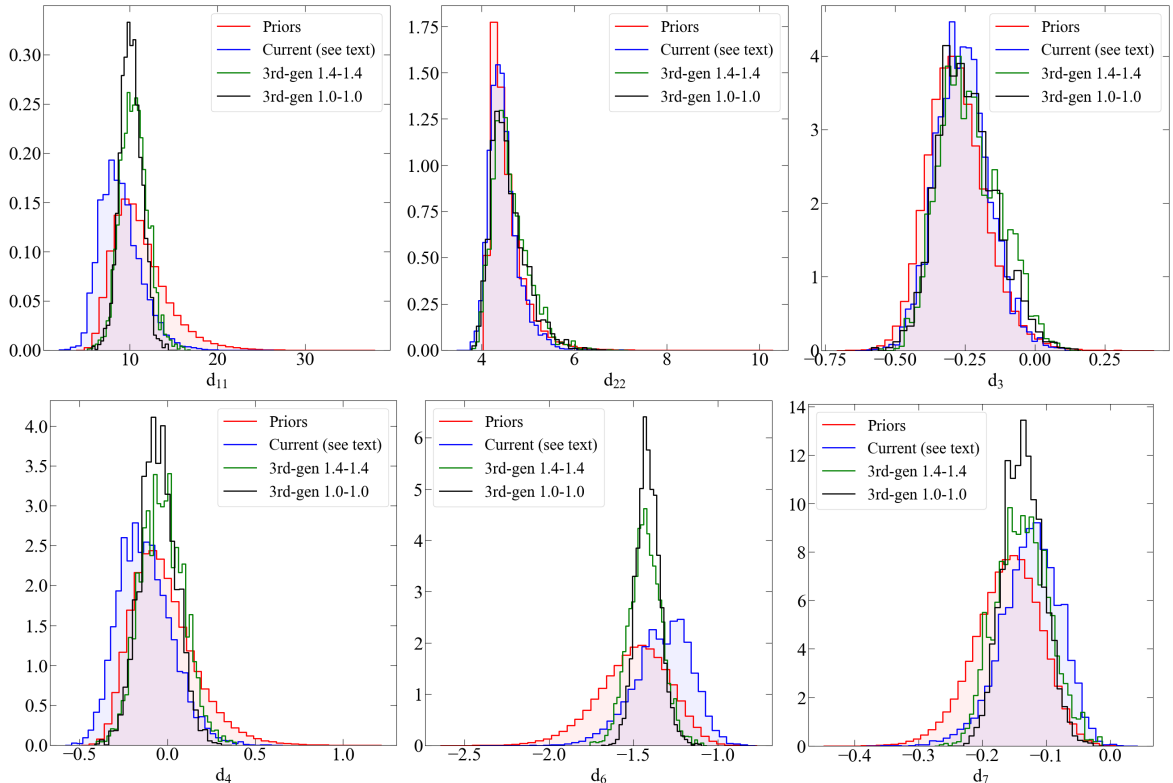


FIG. 1. Priors (red) and posteriors of the analysis of astrophysical data for all six spectral LECs in neutron matter. The priors are results of fits to NN scattering data. The posterior for current astrophysical data includes gravitational-wave, maximum-mass, and NICER data (blue). We also show posteriors from analyses of simulated signals as expected to be observed by third-generation detectors for symmetric binaries with component masses of $1.0M_{\odot}$ (black) and $1.4M_{\odot}$ (green).

burden is essential.

Recent works have taken first steps in this direction. Refs. [39, 40] obtained constraints on a simplified Hamiltonian with a single free parameter representing the strength of a phenomenological 3N force from NS observations. However, a connection to 3N forces from EFT and the possible existence of non-nucleonic degrees of freedom at high densities were not addressed in that work. This was overcome in Ref. [42] where the two pion-nucleon LECs that determine the strength of chiral 3N forces in neutron matter at $N^2\text{LO}$ were studied using a more flexible EOS model. In both works, broad uniform prior distributions on the 3N LECs were employed and canonical constraints from nuclear experiments, such as NN scattering data analyzed consistently with EFT truncation uncertainties, were not taken into account.

Here, we overcome these limitations and study the impact of NS observations on all unknown LECs in an $N^2\text{LO}$ Hamiltonian in neutron matter, rather than limiting ourselves to the 3N sector. We achieve this by combining our previously developed emulators [52] for auxiliary-field diffusion Monte Carlo (AFDMC) [53, 54] calculations of neutron matter and for the TOV equations [51] to establish a direct connection of the LECs at $N^2\text{LO}$ with NS properties. As the long-range pion-nucleon LECs are very tightly constrained from experimental data [55, 56],

we keep them fixed in this work. Then, the 3N sector in neutron matter is parameter-free at this order [32], and we effectively study the contact sector of the NN force. This allows us to analyze the interplay between NN scattering data and NS observations in constraining the Hamiltonian.

We employ both of our emulators to sample over the LECs when analyzing NS data and performing GW inference with PyCBC [57]. Prior information from NN scattering data is incorporated in a hierarchical manner within PyCBC by implementing LEC posteriors from a scattering analysis [12] as GW priors. We present our main results in Fig. 1, and find that present astrophysical data provide slight constraints on the relevant spectral LECs at $N^2\text{LO}$ if nuclear Hamiltonians are used up to $2n_0$. We also study the potential of next-generation GW detectors and find that these observatories can provide strong constraints on LECs, highlighting their high discovery potential for nuclear physics.

Emulators for Dense Matter. For a given Hamiltonian with a specified set of LECs, we employ AFDMC to calculate the EOS of pure neutron matter. AFDMC provides very accurate and precise solutions to the quantum many-body problem but at a significant computational cost. We have employed the parametric matrix model (PMM) [58] to build emulators for AFDMC calculations

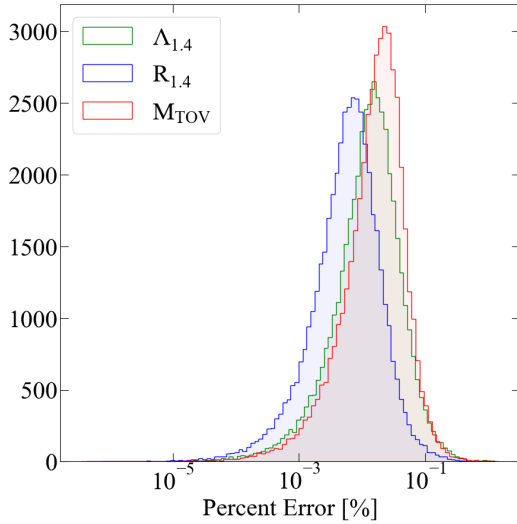


FIG. 2. Percent error of the MLP neural network emulators for M_{TOV} (red), the radius (blue), and the tidal deformability (green) of a $1.4M_{\odot}$ neutron star. In all panels, we show histograms for 70,000 validation samples.

of pure neutron matter for local chiral EFT Hamiltonians at $N^2\text{LO}$ [52]. The PMM is based off of the reduced-basis method (RBM) [59–65] which identifies a relevant low-dimensional subspace that contains the solution space as the LECs in the Hamiltonian are varied. While the RBM explicitly calculates this subspace from high-fidelity solutions to the problem at hand, the PMM identifies this subspace implicitly through fitting matrix elements in a representative low-dimensional matrix equation directly to the AFDMC data. This equation is set up as an eigenvalue problem for a matrix \hat{H} with the same structure as the chiral EFT Hamiltonian:

$$\hat{H} = H_0 + d_1 \cdot H_1 + d_2 \cdot H_2 + \dots, \quad (1)$$

where the d_i are the LECs of the Hamiltonian, and e.g., in the 2-dimensional case,

$$\begin{aligned} \hat{H} &= \begin{bmatrix} \alpha & \beta \\ \beta & \gamma \end{bmatrix}, H_0 = \begin{bmatrix} a & 0 \\ 0 & b \end{bmatrix}, \\ H_1 &= \begin{bmatrix} c & d \\ d & e \end{bmatrix}, H_2 = \begin{bmatrix} f & g \\ g & h \end{bmatrix}, \end{aligned} \quad (2)$$

with real matrix elements $a - h$. These matrix elements are constrained by fitting the lowest eigenvalue of \hat{H} to AFDMC energies in neutron matter for ~ 30 training LEC sets. At $N^2\text{LO}$, there are nine operator LECs describing NN forces, but only six combinations of these operator LECs, i.e. spectral LECs, contribute to pure neutron matter. The emulator is set up with the six relevant spectral LECs d_i . The 3N forces are fixed because, in neutron matter, they only depend on pion-nucleon LECs at $N^2\text{LO}$.

The emulators developed in Ref. [52] allow us to speed up AFDMC calculations by a factor of 10^8 while maintaining errors around 1%, which is comparable to the

statistical uncertainty of AFDMC [53]. This dramatic reduction of computational cost enables us to perform Bayesian inference. More details on our PMM emulator can be found in Ref. [52].

Neutron-Star Equations of State. For a given set of LECs, the PMM allows us to calculate the neutron-matter energy per particle at $0.12, 0.16, 0.24, 0.32, 0.48 \text{ fm}^{-3}$. We then use the nuclear meta-model [66, 67] to extend the PMM output to neutron-star matter. The metamodel describes the energy per particle of nuclear matter at various densities and asymmetries in terms of the nuclear empirical parameters (NEPs), defined by Taylor expansions of the energy per particle in symmetric nuclear matter and of the symmetry energy.

We first generate a set of symmetric-matter parameters. We fix $E_{\text{sat}} = -16 \text{ MeV}$ and $n_{\text{sat}} = 0.16 \text{ fm}^{-3}$, and sample K_{sat} , Q_{sat} , and Z_{sat} from the following Gaussian distributions: $K_{\text{sat}} = 227 \pm 18 \text{ MeV}$, $Q_{\text{sat}} = -172 \pm 243 \text{ MeV}$, and $Z_{\text{sat}} = 1287 \pm 1499 \text{ MeV}$ [68]. We then sample a set of six spectral LECs $d_{11}, d_{22}, d_3, d_4, d_6$, and d_7 from the posteriors of Ref. [12], and use the PMM to generate a neutron-matter EOS. With both curves specified, we fit the meta-model, and generate an EOS in beta equilibrium. For all models, we attach the crust of Douchin and Haensel [69] below 0.08 fm^{-3} following the approach outlined in Ref. [70]. Therefore, each meta-model EOS depends on a set of 9 parameters.

Because we cannot expect the nucleonic description of dense matter to be valid at the highest densities reached in the cores of NSs, we transition from the meta-model to a speed-of-sound extension [71–73] at a transition density $n_{\text{tr}} = 2n_0$. We sample values of the squared speed of sound, c_i^2 , uniformly between 10^{-5} and 1 on a density grid ranging from $3n_0$ to $6n_0$ in steps of n_0 . We then connect these points by linear speed-of-sound segments and choose the speed of sound to be constant after the last density point. Finally, we connect the speed-of-sound model to the meta model and construct the EOS at all densities up to $12n_0$. Each final EOS is, therefore, described by a total of 13 parameters.

Emulators for neutron-star structure. To build emulators for the TOV equations, we follow Ref. [51] and employ multilayer-perceptron (MLP) neural networks. We generate mass-radius and mass-tidal-deformability curves for 270,000 EOS, and split these into a training set (200,000 EOS) and a validation set (70,000 EOS). We remove all samples with a maximum NS mass $M_{\text{TOV}} < 2M_{\odot}$ because the observations of heavy pulsars with masses greater than $2M_{\odot}$ rule these EOS out. We then build three separate MLP networks to respectively emulate M_{TOV} , the radii $r(m)$, and the tidal deformabilities $\Lambda(m)$. Each MLP emulator takes the 13 parameters describing each EOS as input.

To emulate M_{TOV} , we train an MLP regressor to the M_{TOV} of our training EOS. For the validation set, our emulator predicts M_{TOV} with errors of $\sim 0.01\%$, see Fig. 2. To build emulators for the radii and tidal deformabilities, we define a mass grid of 30 uniformly spaced

points between $1M_{\odot}$ and M_{TOV} for each of the training EOS. Two MLP regressors are then trained on the radii and the logarithm of the tidal deformabilities at the grid points, respectively. For any new parameter set, we first predict M_{TOV} and then use the other emulators to infer radii and tidal deformabilities at the mass-grid points. We find that these emulators perform extremely well, with speed ups of two orders of magnitude [51] and errors around 0.01% over the validation set, see Fig. 2 for the error distributions for both quantities at $1.4M_{\odot}$. We show example outputs in the Supplemental Material.

Multimessenger Data Analysis. Recent years have seen a wealth of new NS data. Radio observations of heavy pulsars have firmly established the existence of two-solar-mass NSs [43–45]. The first gravitational-wave (GW) observation of a binary NS merger, GW170817 [46], constrained the tidal deformability for a $1.4M_{\odot}$ NS to be 190^{+390}_{-120} at the 90% credible level [74], implying the EOS to be rather soft up to $(3 - 4)n_0$. Finally, NICER has measured the masses and radii of four pulsars [47–50].

To analyze GW170817 data, we follow Ref. [57] to implement the MLP networks in the PyCBC GW Bayesian analysis software. We compute the posterior $p(\vec{\theta}|d(t), H)$ by sampling over the parameters $\vec{\theta}$ that enter the waveform model H , for which we choose the SEOBNRv4T-surrogate template [75]. The parameters $\vec{\theta}$ are the 13 parameters that describe the EOS as well as the parameters describing the binary system. For the EOS parameters, we use our emulators to predict $r(m)$ and $\Lambda(m)$ between $1.0M_{\odot}$ and M_{TOV} . As in Ref. [57], we fix the sky and distance parameters to the ones for GW170817 [76, 77] and sample the source frame chirp mass $\mathcal{M}_c^{\text{src}}$, mass ratio q , offset of trigger time Δt_c , inclination angle ι , and the two NS spins $\chi_{1z,2z}$, and marginalize the polarization angle and phase using a uniform prior from $[0, 2\pi]$ for both. We compare the predicted waveform to the strain data $d(t)$ measured by the LIGO Hanford, LIGO Livingston, and Virgo detectors [78, 79], by employing PyCBC Inference [80] and sample using the EMCEE Markov Chain Monte Carlo (MCMC) sampler. The inference calls the emulator via a plug-in waveform model developed in Ref. [57].

In Fig. 3, we show 9800 mass-radius relations drawn from the GW posterior of our PyCBC analysis. The main effect of the GW data is to rule out stiffer EOS, consistent with previous analyses [42, 46, 81–87]. We further apply the maximum-mass constraint by comparing the predicted M_{max} for each EOS to the observed neutron star masses [70]. The likelihood is dominated by PSR J0740+6620 [45] with a mass of $2.08 \pm 0.07 M_{\odot}$. Finally, we apply mass-radius constraints from the four NICER pulsars PSR J0030+0451 [47], PSR J0740+6620 [48], PSR J0437–4715 [49], and PSR J0614–3329 [50]. For the first two pulsars, independent results have been provided by the Maryland group of the NICER collaboration [85, 88]. Given all sources of data, we can put tight constraints on the NS mass-radius relation. We find the radius of a $1.4M_{\odot}$ NS to be $11.6^{+0.7}_{-0.5}\text{km}$ at the 90% cred-

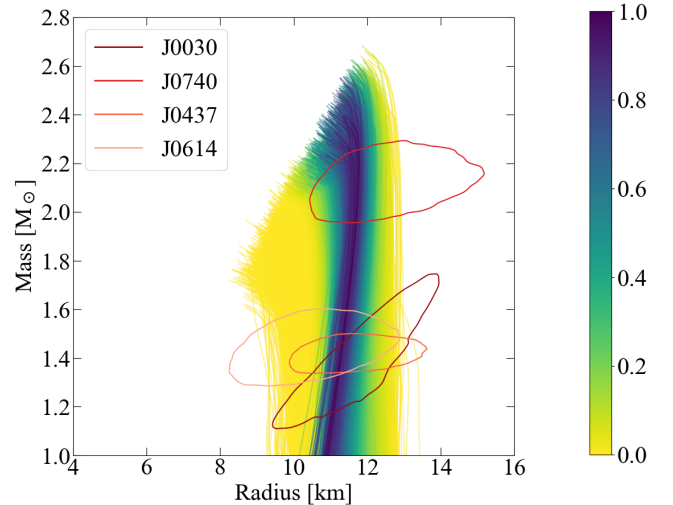


FIG. 3. Mass-radius curves drawn from the GW posterior where the maximum-mass and NICER likelihoods are applied. The EOS are colored according to their posterior probability normalized to the highest value. We also show the four NICER contours at 95% credible level.

ible level.

Constraining Nuclear Interactions. Because we sample over the EOS parameters during the data analysis, we can directly infer the LECs from multi-messenger observations of NSs and their mergers. We present our results for the LECs given present astrophysical observations in Fig. 1 and find that current NS data provides modest information on some spectral LECs. While the distributions of the LECs that enter PNM through their contribution to singlet S -wave interactions (d_{22} and d_3) [89] remain nearly unchanged, the distributions of the LECs entering the triplet P -wave channels (d_{11}, d_4, d_6 , and d_7) undergo moderate change after the inference is performed. The astrophysical data reduces P -wave repulsion, which is in line with NS data preferring softer EOS. This is driven by both GW and NICER data which pull the LEC posteriors in the same direction, see the Supplemental Material. As a consequence, even present NS observations provide information on NN forces in the nuclear Hamiltonian, beyond what is provided by scattering data.

Impact of Future Detectors. Future observations, for example by next-generation GW detectors such as Cosmic Explorer [90, 91] or the Einstein Telescope [92, 93], will provide additional precision data that allows us to further constrain the LECs. To demonstrate this, we inject two simulated events into a detector network composed of two Cosmic Explorer interferometers and one Einstein Telescope. For both events, we chose most of the injection parameter values consistent with those that were inferred for GW170817. For the first event, the two component masses were taken to be $1.4 M_{\odot}$, leading to

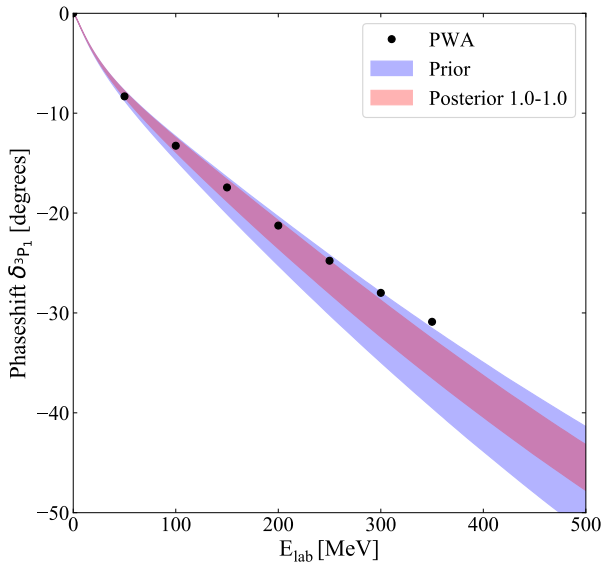


FIG. 4. Phase shifts for the 3P_1 partial wave at the 90% CI for the prior (blue) and the posterior obtained from the analysis of the $1.0 - 1.0 M_{\odot}$ injection (red). We also show the results of the Nijmegen partial-wave analysis [94] for comparison (black).

an SNR of ~ 2300 . For the second event, the two component masses were decreased to $1.0 M_{\odot}$ to probe the sensitivity of the LECs to the NS masses. This event was found to have an SNR of ~ 1730 . The injected LEC values were chosen to be close to the 50th percentiles of the corresponding prior distributions. The obtained posteriors for the LECs are also shown in Fig. 1. We find that next-generation GW detectors can provide significant constraints on the LECs for these two events. Interestingly, the LECs are better constrained for the lower SNR (low-mass) event as it probes lower densities that are closer to the regime described by chiral EFT.

Finally, for these next-generation posteriors, we re-examine the phase shifts in the triplet P -wave channels. We find no changes to the phase shift in the 3P_0 partial wave and marginal changes in the 3P_2 channel with respect to the priors. However, we observe a clear change in the 3P_1 channel mainly at high energies $\gtrsim 200$ MeV, see Fig. 4. This channel is repulsive and leads to the largest

of the P -wave phase shifts whereas 3P_0 and 3P_2 are both attractive and smaller in magnitude. As we found before, the data seems to overall reduce P -wave repulsion. This analysis serves as an important sensitivity study which demonstrates that, among the triplet P waves, the 3P_1 channel is more strongly correlated with the properties of NSs. In addition, the fact that the spectral LECs change considerably after next-generation data is included while the phase shift bands change only moderately shows that astrophysical data provides complementary information when compared to NN scattering.

Summary and Outlook. In this work, we have used emulators based on the PMM and MLP machine-learning frameworks to constrain the relevant two-nucleon LECs in an N^2LO chiral EFT Hamiltonian from NS data. We found that current observations only provide mild constraints in addition to two-nucleon scattering measured in the lab, but that next-generation GW observatories provide strong and complimentary information on microscopic LECs. Our pipeline paves the way of measuring LECs that are difficult to extract from laboratory data.

ACKNOWLEDGMENTS

This work was supported by the U.S. Department of Energy through Los Alamos National Laboratory (LANL). LANL is operated by Triad National Security, LLC, for the National Nuclear Security Administration of U.S. Department of Energy (Contract No. 89233218CNA000001). C.L.A., B.T.R., S.D., R.S., and I.T. were supported by the Laboratory Directed Research and Development (LDRD) program of LANL under project number 20230315ER. C.L.A., R.S., and I.T. were also supported by the LDRD program of LANL under project number 20260260ER. C.L.A. and B.T.R. were also supported by LANL through its Center for Space and Earth Science, which is funded by LANL's LDRD program under project number 20240477CR. B.T.R. and I.T. were also supported by the U.S. Department of Energy, Office of Science, Office of Nuclear Physics program under Award Number DE-SCL0000015. S.D. was also supported by the Laboratory Directed Research and Development program of Los Alamos National Laboratory project 20250750ECR.

[1] J. M. Lattimer and M. Prakash, The physics of neutron stars, *Science* **304**, 536 (2004), arXiv:astro-ph/0405262.

[2] A. L. Watts *et al.*, Colloquium : Measuring the neutron star equation of state using x-ray timing, *Rev. Mod. Phys.* **88**, 021001 (2016), arXiv:1602.01081 [astro-ph.HE].

[3] K. Chatzioannou, H. T. Cromartie, S. Gandolfi, I. Tews, D. Radice, A. W. Steiner, and A. L. Watts, Neutron stars and the dense matter equation of state: from microscopic theory to macroscopic observations, arXiv:2407.11153 [nucl-th] (2024).

[4] E. Epelbaum, H.-W. Hammer, and U.-G. Meissner, Modern Theory of Nuclear Forces, *Rev. Mod. Phys.* **81**, 1773 (2009), arXiv:0811.1338 [nucl-th].

[5] R. Machleidt and D. R. Entem, Chiral effective field theory and nuclear forces, *Phys. Rept.* **503**, 1 (2011), arXiv:1105.2919 [nucl-th].

[6] D. R. Entem and R. Machleidt, Accurate charge dependent nucleon nucleon potential at fourth order of chiral perturbation theory, *Phys. Rev. C* **68**, 041001 (2003),

arXiv:nucl-th/0304018.

[7] E. Epelbaum, W. Glockle, and U.-G. Meissner, The Two-nucleon system at next-to-next-to-next-to-leading order, *Nucl. Phys. A* **747**, 362 (2005), arXiv:nucl-th/0405048.

[8] A. Gezerlis, I. Tews, E. Epelbaum, S. Gandolfi, K. Hebeler, A. Nogga, and A. Schwenk, Quantum Monte Carlo Calculations with Chiral Effective Field Theory Interactions, *Phys. Rev. Lett.* **111**, 032501 (2013), arXiv:1303.6243 [nucl-th].

[9] M. Piarulli, L. Girlanda, R. Schiavilla, R. Navarro Pérez, J. E. Amaro, and E. Ruiz Arriola, Minimally nonlocal nucleon-nucleon potentials with chiral two-pion exchange including Δ resonances, *Phys. Rev. C* **91**, 024003 (2015), arXiv:1412.6446 [nucl-th].

[10] P. Reinert, H. Krebs, and E. Epelbaum, Semilocal momentum-space regularized chiral two-nucleon potentials up to fifth order, *Eur. Phys. J. A* **54**, 86 (2018), arXiv:1711.08821 [nucl-th].

[11] D. R. Entem, R. Machleidt, and Y. Nosyk, High-quality two-nucleon potentials up to fifth order of the chiral expansion, *Phys. Rev. C* **96**, 024004 (2017), arXiv:1703.05454 [nucl-th].

[12] R. Somasundaram, J. E. Lynn, L. Huth, A. Schwenk, and I. Tews, Maximally local two-nucleon interactions at N3LO in Δ -less chiral effective field theory, *Phys. Rev. C* **109**, 034005 (2024), arXiv:2306.13579 [nucl-th].

[13] P. Navratil, V. G. Gueorguiev, J. P. Vary, W. E. Ormand, and A. Nogga, Structure of $A=10-13$ nuclei with two plus three-nucleon interactions from chiral effective field theory, *Phys. Rev. Lett.* **99**, 042501 (2007), arXiv:nucl-th/0701038.

[14] D. Gazit, S. Quaglioni, and P. Navratil, Three-Nucleon Low-Energy Constants from the Consistency of Interactions and Currents in Chiral Effective Field Theory, *Phys. Rev. Lett.* **103**, 102502 (2009), [Erratum: *Phys. Rev. Lett.* 122, 029901 (2019)], arXiv:0812.4444 [nucl-th].

[15] K. Hebeler, S. K. Bogner, R. J. Furnstahl, A. Nogga, and A. Schwenk, Improved nuclear matter calculations from chiral low-momentum interactions, *Phys. Rev. C* **83**, 031301 (2011), arXiv:1012.3381 [nucl-th].

[16] J. E. Lynn, I. Tews, J. Carlson, S. Gandolfi, A. Gezerlis, K. E. Schmidt, and A. Schwenk, Chiral Three-Nucleon Interactions in Light Nuclei, Neutron- α Scattering, and Neutron Matter, *Phys. Rev. Lett.* **116**, 062501 (2016), arXiv:1509.03470 [nucl-th].

[17] M. Piarulli *et al.*, Light-nuclei spectra from chiral dynamics, *Phys. Rev. Lett.* **120**, 052503 (2018), arXiv:1707.02883 [nucl-th].

[18] E. Epelbaum *et al.* (LENPIC), Few- and many-nucleon systems with semilocal coordinate-space regularized chiral two- and three-body forces, *Phys. Rev. C* **99**, 024313 (2019), arXiv:1807.02848 [nucl-th].

[19] I. Tews, R. Somasundaram, D. Lonardoni, H. Göttling, R. Seutin, J. Carlson, S. Gandolfi, K. Hebeler, and A. Schwenk, Neutron matter from local chiral effective field theory interactions at large cutoffs, *Phys. Rev. Res.* **7**, 033024 (2025), arXiv:2407.08979 [nucl-th].

[20] R. Curry, K. Hebeler, S. Gandolfi, A. Gezerlis, A. Schwenk, R. Somasundaram, and I. Tews, Quantum Monte Carlo Calculations of Light Nuclei with Fully Propagated Theoretical Uncertainties, arXiv:2510.15860 [nucl-th] (2025).

[21] A. Ekström, G. R. Jansen, K. A. Wendt, G. Hagen, T. Papenbrock, B. D. Carlsson, C. Forssén, M. Hjorth-Jensen, P. Navrátil, and W. Nazarewicz, Accurate nuclear radii and binding energies from a chiral interaction, *Phys. Rev. C* **91**, 051301 (2015), [Erratum: *Phys. Rev. C* 109, 059901 (2024)], arXiv:1502.04682 [nucl-th].

[22] P. Arthuis, K. Hebeler, and A. Schwenk, Neutron-rich nuclei and neutron skins from chiral low-resolution interactions, arXiv:2401.06675 [nucl-th] (2024).

[23] S. R. Stroberg, J. D. Holt, A. Schwenk, and J. Simonis, *Ab Initio* Limits of Atomic Nuclei, *Phys. Rev. Lett.* **126**, 022501 (2021), arXiv:1905.10475 [nucl-th].

[24] T. Miyagi, S. R. Stroberg, P. Navrátil, K. Hebeler, and J. D. Holt, Converged ab initio calculations of heavy nuclei, *Phys. Rev. C* **105**, 014302 (2022), arXiv:2104.04688 [nucl-th].

[25] B. Hu *et al.*, Ab initio predictions link the neutron skin of ^{208}Pb to nuclear forces, *Nature Phys.* **18**, 1196 (2022), arXiv:2112.01125 [nucl-th].

[26] K. Hebeler, V. Durant, J. Hoppe, M. Heinz, A. Schwenk, J. Simonis, and A. Tichai, Normal ordering of three-nucleon interactions for ab initio calculations of heavy nuclei, *Phys. Rev. C* **107**, 024310 (2023), arXiv:2211.16262 [nucl-th].

[27] T. Miyagi, X. Cao, R. Seutin, S. Bacca, R. F. Garcia Ruiz, K. Hebeler, J. D. Holt, and A. Schwenk, Impact of Two-Body Currents on Magnetic Dipole Moments of Nuclei, *Phys. Rev. Lett.* **132**, 232503 (2024), arXiv:2311.14383 [nucl-th].

[28] M. Door *et al.*, Probing New Bosons and Nuclear Structure with Ytterbium Isotope Shifts, *Phys. Rev. Lett.* **134**, 063002 (2025), arXiv:2403.07792 [physics.atom-ph].

[29] F. Bonaiti, G. Hagen, and T. Papenbrock, Structure of the doubly magic nuclei ^{208}Pb and ^{266}Pb from ab initio computations, arXiv:2508.14217 [nucl-th] (2025).

[30] Z. Li, T. Miyagi, and A. Schwenk, Ab initio calculations of beta-decay half-lives for $N = 50$ neutron-rich nuclei, arXiv:2509.06812 [nucl-th] (2025).

[31] J. Kuske, T. Miyagi, A. Arcones, and A. Schwenk, r-process nucleosynthesis with ab initio nuclear masses around the $N=82$ shell closure, arXiv:2509.19131 [astro-ph.HE] (2025).

[32] K. Hebeler and A. Schwenk, Chiral three-nucleon forces and neutron matter, *Phys. Rev. C* **82**, 014314 (2010), arXiv:0911.0483 [nucl-th].

[33] I. Tews, T. Krüger, K. Hebeler, and A. Schwenk, Neutron matter at next-to-next-to-next-to-leading order in chiral effective field theory, *Phys. Rev. Lett.* **110**, 032504 (2013), arXiv:1206.0025 [nucl-th].

[34] C. Drischler, K. Hebeler, and A. Schwenk, Chiral interactions up to next-to-next-to-next-to-leading order and nuclear saturation, *Phys. Rev. Lett.* **122**, 042501 (2019), arXiv:1710.08220 [nucl-th].

[35] C. Drischler, J. A. Melendez, R. J. Furnstahl, and D. R. Phillips, Quantifying uncertainties and correlations in the nuclear-matter equation of state, *Phys. Rev. C* **102**, 054315 (2020), arXiv:2004.07805 [nucl-th].

[36] A. Lovato, I. Bombaci, D. Logoteta, M. Piarulli, and R. B. Wiringa, Benchmark calculations of infinite neutron matter with realistic two- and three-nucleon potentials, *Phys. Rev. C* **105**, 055808 (2022), arXiv:2202.10293 [nucl-th].

[37] J. Keller, K. Hebeler, and A. Schwenk, Nuclear Equation of State for Arbitrary Proton Fraction and Temperature Based on Chiral Effective Field Theory and a Gaussian Process Emulator, *Phys. Rev. Lett.* **130**, 072701 (2023),

arXiv:2204.14016 [nucl-th].

[38] F. Marino, W. Jiang, and S. J. Novario, Diagrammatic ab initio methods for infinite nuclear matter with modern chiral interactions, *Phys. Rev. C* **110**, 054322 (2024), arXiv:2407.17098 [nucl-th].

[39] A. Maselli, A. Sabatucci, and O. Benhar, Constraining three-nucleon forces with multimessenger data, *Phys. Rev. C* **103**, 065804 (2021), arXiv:2010.03581 [astro-ph.HE].

[40] A. Sabatucci, O. Benhar, A. Maselli, and C. Pacilio, Sensitivity of neutron star observations to three-nucleon forces, *Phys. Rev. D* **106**, 083010 (2022), arXiv:2206.11286 [astro-ph.HE].

[41] H. Rose, N. Kunert, T. Dietrich, P. T. H. Pang, R. Smith, C. Van Den Broeck, S. Gandolfi, and I. Tews, Revealing the strength of three-nucleon interactions with the proposed Einstein Telescope, *Phys. Rev. C* **108**, 025811 (2023), arXiv:2303.11201 [astro-ph.HE].

[42] R. Somasundaram, I. Svensson, S. De, A. E. Deneris, Y. Dietz, P. Landry, A. Schwenk, and I. Tews, Inferring three-nucleon couplings from multi-messenger neutron-star observations, *Nature Commun.* **16**, 9819 (2025), arXiv:2410.00247 [nucl-th].

[43] J. Antoniadis *et al.*, A Massive Pulsar in a Compact Relativistic Binary, *Science* **340**, 6131 (2013), arXiv:1304.6875 [astro-ph.HE].

[44] Z. Arzoumanian *et al.* (NANOGrav), The NANOGrav 11-year Data Set: High-precision timing of 45 Millisecond Pulsars, *Astrophys. J. Suppl.* **235**, 37 (2018), arXiv:1801.01837 [astro-ph.HE].

[45] E. Fonseca *et al.*, Refined Mass and Geometric Measurements of the High-mass PSR J0740+6620, *Astrophys. J. Lett.* **915**, L12 (2021), arXiv:2104.00880 [astro-ph.HE].

[46] B. P. Abbott *et al.* (LIGO Scientific, Virgo), GW170817: Observation of Gravitational Waves from a Binary Neutron Star Inspiral, *Phys. Rev. Lett.* **119**, 161101 (2017), arXiv:1710.05832 [gr-qc].

[47] S. Vinciguerra *et al.*, An Updated Mass–Radius Analysis of the 2017–2018 NICER Data Set of PSR J0030+0451, *Astrophys. J.* **961**, 62 (2024), arXiv:2308.09469 [astro-ph.HE].

[48] T. Salmi *et al.*, The Radius of the High-mass Pulsar PSR J0740+6620 with 3.6 yr of NICER Data, *Astrophys. J.* **974**, 294 (2024), arXiv:2406.14466 [astro-ph.HE].

[49] D. Choudhury *et al.*, A NICER View of the Nearest and Brightest Millisecond Pulsar: PSR J0437–4715, *Astrophys. J. Lett.* **971**, L20 (2024), arXiv:2407.06789 [astro-ph.HE].

[50] L. Mauviard *et al.*, A NICER view of the 1.4 solar-mass edge-on pulsar PSR J0614–3329, arXiv:2506.14883 [astro-ph.HE] (2025).

[51] B. T. Reed, R. Somasundaram, S. De, C. L. Armstrong, P. Giuliani, C. Capano, D. A. Brown, and I. Tews, Toward Accelerated Nuclear-physics Parameter Estimation from Binary Neutron Star Mergers: Emulators for the Tolman–Oppenheimer–Volkoff Equations, *Astrophys. J.* **974**, 285 (2024), arXiv:2405.20558 [astro-ph.HE].

[52] C. L. Armstrong, P. Giuliani, K. Godbey, R. Somasundaram, and I. Tews, Emulators for Scarce and Noisy Data: Application to Auxiliary-Field Diffusion Monte Carlo for Neutron Matter, *Phys. Rev. Lett.* **135**, 142501 (2025), arXiv:2502.03680 [nucl-th].

[53] J. Carlson, S. Gandolfi, F. Pederiva, S. C. Pieper, R. Schiavilla, K. E. Schmidt, and R. B. Wiringa, Quantum Monte Carlo methods for nuclear physics, *Rev. Mod. Phys.* **87**, 1067 (2015), arXiv:1412.3081 [nucl-th].

[54] J. E. Lynn, I. Tews, S. Gandolfi, and A. Lovato, Quantum Monte Carlo Methods in Nuclear Physics: Recent Advances, *Ann. Rev. Nucl. Part. Sci.* **69**, 279 (2019), arXiv:1901.04868 [nucl-th].

[55] M. Hoferichter, J. Ruiz de Elvira, B. Kubis, and U.-G. Meißner, Roy–Steiner-equation analysis of pion–nucleon scattering, *Phys. Rept.* **625**, 1 (2016), arXiv:1510.06039 [hep-ph].

[56] D. Siemens, J. Ruiz de Elvira, E. Epelbaum, M. Hoferichter, H. Krebs, B. Kubis, and U. G. Meißner, Reconciling threshold and subthreshold expansions for pion–nucleon scattering, *Phys. Lett. B* **770**, 27 (2017), arXiv:1610.08978 [nucl-th].

[57] B. T. Reed, C. L. Armstrong, R. Somasundaram, C. Capano, S. De, and I. Tews, Direct Inference of Nuclear Equation-of-State Parameters from Gravitational-Wave Observations, arXiv:2506.15984 [astro-ph.HE] (2025).

[58] P. Cook, D. Jammooa, M. Hjorth-Jensen, D. D. Lee, and D. Lee, Parametric Matrix Models, arXiv:2401.11694 [cs.LG] (2024).

[59] D. Frame, R. He, I. Ipsen, D. Lee, D. Lee, and E. Rrapaj, Eigenvector continuation with subspace learning, *Phys. Rev. Lett.* **121**, 032501 (2018).

[60] S. König, A. Ekström, K. Hebeler, D. Lee, and A. Schwenk, Eigenvector continuation as an efficient and accurate emulator for uncertainty quantification, *Physics Letters B* **810**, 135814 (2020), arXiv:1909.08446 [nucl-th].

[61] E. Bonilla, P. Giuliani, K. Godbey, and D. Lee, Training and projecting: A reduced basis method emulator for many-body physics, *Phys. Rev. C* **106**, 054322 (2022), arXiv:2203.05284 [nucl-th].

[62] C. Drischler, J. A. Melendez, R. J. Furnstahl, A. J. Garcia, and X. Zhang, BUQEYE guide to projection-based emulators in nuclear physics, *Front. in Phys.* **10**, 1092931 (2022), arXiv:2212.04912 [nucl-th].

[63] J. A. Melendez, C. Drischler, R. J. Furnstahl, A. J. Garcia, and X. Zhang, Model reduction methods for nuclear emulators, *J. Phys. G* **49**, 102001 (2022), arXiv:2203.05528 [nucl-th].

[64] T. Duguet, A. Ekström, R. J. Furnstahl, S. König, and D. Lee, Colloquium: Eigenvector continuation and projection-based emulators, *Rev. Mod. Phys.* **96**, 031002 (2024), arXiv:2310.19419 [nucl-th].

[65] P. Giuliani, K. Godbey, E. Bonilla, F. Viens, and J. Piekarewicz, Bayes goes fast: Uncertainty quantification for a covariant energy density functional emulated by the reduced basis method, *Frontiers in Physics* **10**, 1054524 (2023), arXiv:2209.13039 [nucl-th].

[66] J. Margueron, R. Hoffmann Casali, and F. Gulminelli, Equation of state for dense nucleonic matter from meta-modeling. I. Foundational aspects, *Phys. Rev. C* **97**, 025805 (2018), arXiv:1708.06894 [nucl-th].

[67] J. Margueron, R. Hoffmann Casali, and F. Gulminelli, Equation of state for dense nucleonic matter from meta-modeling. II. Predictions for neutron star properties, *Phys. Rev. C* **97**, 025806 (2018), arXiv:1708.06895 [nucl-th].

[68] R. Somasundaram, C. Drischler, I. Tews, and J. Margueron, Constraints on the nuclear symmetry energy from asymmetric-matter calculations with chiral NN and $3N$ interactions, *Phys. Rev. C* **103**, 045803 (2021), arXiv:2009.04737 [nucl-th].

[69] F. Douchin and P. Haensel, A unified equation of state of dense matter and neutron star structure, *Astron. Astrophys.* **380**, 151 (2001), arXiv:astro-ph/0111092.

[70] H. Koehn *et al.*, From existing and new nuclear and astrophysical constraints to stringent limits on the equation of state of neutron-rich dense matter, *Phys. Rev. X* **15**, 021014 (2025), arXiv:2402.04172 [astro-ph.HE].

[71] I. Tews, J. Margueron, and S. Reddy, Critical examination of constraints on the equation of state of dense matter obtained from GW170817, *Phys. Rev. C* **98**, 045804 (2018), arXiv:1804.02783 [nucl-th].

[72] S. K. Greif, G. Raaijmakers, K. Hebeler, A. Schwenk, and A. L. Watts, Equation of state sensitivities when inferring neutron star and dense matter properties, *Mon. Not. Roy. Astron. Soc.* **485**, 5363 (2019), arXiv:1812.08188 [astro-ph.HE].

[73] R. Somasundaram, I. Tews, and J. Margueron, Investigating signatures of phase transitions in neutron-star cores, *Phys. Rev. C* **107**, 025801 (2023), arXiv:2112.08157 [nucl-th].

[74] B. P. Abbott *et al.* (LIGO Scientific, Virgo), GW170817: Measurements of neutron star radii and equation of state, *Phys. Rev. Lett.* **121**, 161101 (2018), arXiv:1805.11581 [gr-qc].

[75] G. Pratten, L. M. Thomas, and A. Ramos Buades, Lal-suite waveform data, 10.5281/zenodo.14999310 (2025).

[76] M. Soares-Santos *et al.* (DES, Dark Energy Camera GW-EM), The Electromagnetic Counterpart of the Binary Neutron Star Merger LIGO/Virgo GW170817. I. Discovery of the Optical Counterpart Using the Dark Energy Camera, *Astrophys. J. Lett.* **848**, L16 (2017), arXiv:1710.05459 [astro-ph.HE].

[77] M. Cantiello *et al.*, A Precise Distance to the Host Galaxy of the Binary Neutron Star Merger GW170817 Using Surface Brightness Fluctuations, *Astrophys. J. Lett.* **854**, L31 (2018), arXiv:1801.06080 [astro-ph.GA].

[78] M. Vallisneri, J. Kanner, R. Williams, A. Weinstein, and B. Stephens, The LIGO Open Science Center, *J. Phys. Conf. Ser.* **610**, 012021 (2015), arXiv:1410.4839 [gr-qc].

[79] R. Abbott *et al.* (LIGO Scientific, Virgo), Open data from the first and second observing runs of Advanced LIGO and Advanced Virgo, *SoftwareX* **13**, 100658 (2021), arXiv:1912.11716 [gr-qc].

[80] C. M. Biwer, C. D. Capano, S. De, M. Cabero, D. A. Brown, A. H. Nitz, and V. Raymond, PyCBC Inference: A Python-based parameter estimation toolkit for compact binary coalescence signals, *Publ. Astron. Soc. Pac.* **131**, 024503 (2019), arXiv:1807.10312 [astro-ph.IM].

[81] E. Annala, T. Gorda, A. Kurkela, and A. Vuorinen, Gravitational-wave constraints on the neutron-star-matter Equation of State, *Phys. Rev. Lett.* **120**, 172703 (2018), arXiv:1711.02644 [astro-ph.HE].

[82] C. D. Capano, I. Tews, S. M. Brown, B. Margalit, S. De, S. Kumar, D. A. Brown, B. Krishnan, and S. Reddy, Stringent constraints on neutron-star radii from multimessenger observations and nuclear theory, *Nature Astron.* **4**, 625 (2020), arXiv:1908.10352 [astro-ph.HE].

[83] T. Dietrich, M. W. Coughlin, P. T. H. Pang, M. Bulla, J. Heinzel, L. Issa, I. Tews, and S. Antier, Multimessenger constraints on the neutron-star equation of state and the Hubble constant, *Science* **370**, 1450 (2020), arXiv:2002.11355 [astro-ph.HE].

[84] R. Essick, I. Tews, P. Landry, and A. Schwenk, Astrophysical Constraints on the Symmetry Energy and the Neutron Skin of Pb208 with Minimal Modeling Assumptions, *Phys. Rev. Lett.* **127**, 192701 (2021), arXiv:2102.10074 [nucl-th].

[85] M. C. Miller *et al.*, The Radius of PSR J0740+6620 from NICER and XMM-Newton Data, *Astrophys. J. Lett.* **918**, L28 (2021), arXiv:2105.06979 [astro-ph.HE].

[86] G. Raaijmakers, S. K. Greif, K. Hebeler, T. Hinderer, S. Nissanke, A. Schwenk, T. E. Riley, A. L. Watts, J. M. Lattimer, and W. C. G. Ho, Constraints on the Dense Matter Equation of State and Neutron Star Properties from NICER’s Mass–Radius Estimate of PSR J0740+6620 and Multimessenger Observations, *Astrophys. J. Lett.* **918**, L29 (2021), arXiv:2105.06981 [astro-ph.HE].

[87] N. Rutherford *et al.*, Constraining the Dense Matter Equation of State with New NICER Mass–Radius Measurements and New Chiral Effective Field Theory Inputs, *Astrophys. J. Lett.* **971**, L19 (2024), arXiv:2407.06790 [astro-ph.HE].

[88] M. C. Miller *et al.*, PSR J0030+0451 Mass and Radius from *NICER* Data and Implications for the Properties of Neutron Star Matter, *Astrophys. J. Lett.* **887**, L24 (2019), arXiv:1912.05705 [astro-ph.HE].

[89] A. Gezerlis, I. Tews, E. Epelbaum, M. Freunek, S. Gandolfi, K. Hebeler, A. Nogga, and A. Schwenk, Local chiral effective field theory interactions and quantum Monte Carlo applications, *Phys. Rev. C* **90**, 054323 (2014), arXiv:1406.0454 [nucl-th].

[90] D. Reitze *et al.*, Cosmic Explorer: The U.S. Contribution to Gravitational-Wave Astronomy beyond LIGO, *Bull. Am. Astron. Soc.* **51**, 035 (2019), arXiv:1907.04833 [astro-ph.IM].

[91] M. Evans *et al.*, A Horizon Study for Cosmic Explorer: Science, Observatories, and Community, arXiv:2109.09882 [astro-ph.IM] (2021).

[92] M. Punturo *et al.*, The Einstein Telescope: A third-generation gravitational wave observatory, *Class. Quant. Grav.* **27**, 194002 (2010).

[93] M. Maggiore *et al.* (ET), Science Case for the Einstein Telescope, *JCAP* **03**, 050, arXiv:1912.02622 [astro-ph.CO].

[94] V. G. J. Stoks, R. A. M. Klomp, M. C. M. Rentmeester, and J. J. de Swart, Partial wave analysis of all nucleon-nucleon scattering data below 350-MeV, *Phys. Rev. C* **48**, 792 (1993).

SUPPLEMENTAL MATERIAL

A. Emulators for TOV

In Fig. 5, we show a set of example mass–radius and mass–tidal-deformability curves from the validation set. We find excellent agreement between the original high-fidelity EOS and the emulator output.

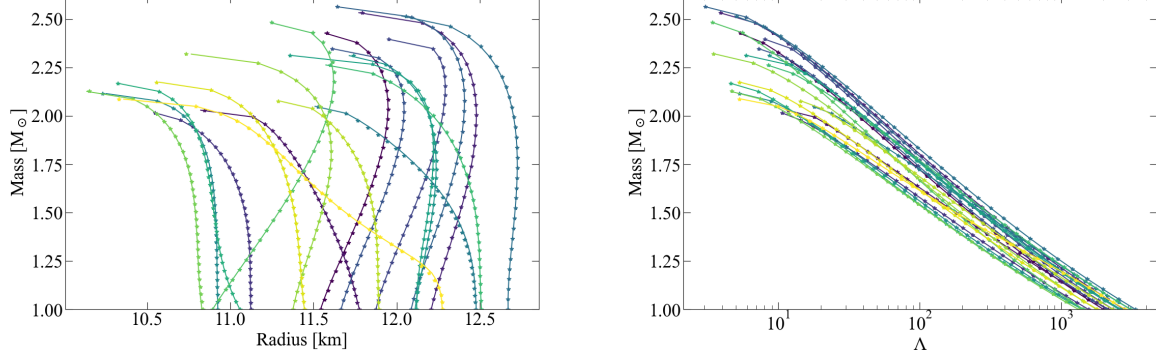


FIG. 5. Examples of solutions to the TOV equations using the high-fidelity solver (lines) and the emulator predictions (points). Left: Mass–radius relations. Right: Mass–tidal-deformability curves.

B. LEC inference at every stage of the analysis

In Fig. 6, we show the results of the LEC inference using current astrophysical data at each step in the analysis, so GW data only, GW and maximum mass data, and finally the full result shown in Fig. 1 of the main manuscript.

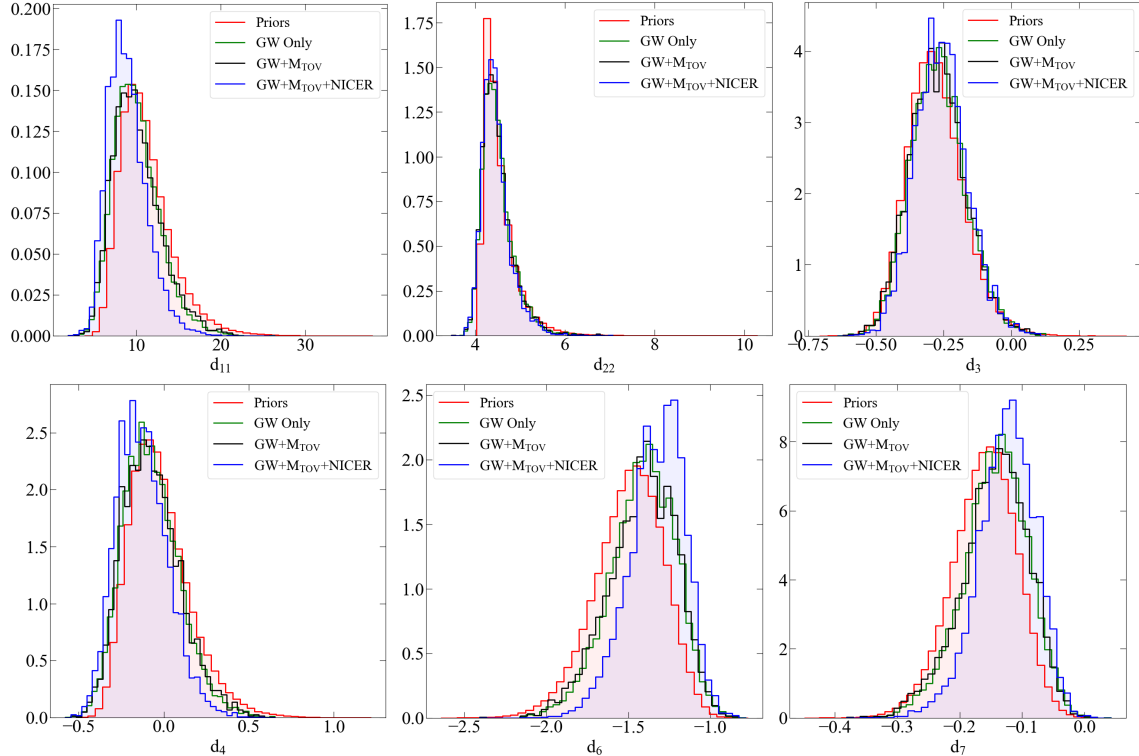


FIG. 6. Priors (red) and posteriors at different stages in the analysis of astrophysical data for all six spectral LECs in neutron matter. The priors are results of fits to NN scattering data. The posteriors include only GW data (green), GW and maximum-mass data (blue), and GW, maximum-mass, and NICER data (blue).